Check for updates

Luminescence

WILEY

LUMINESCENCE
The Journal of Biological and Chemical Luminescence

RESEARCH ARTICLE

Investigation of Carbon Quantum Dots With Good Optical Properties From Sunflower Seed Shells for Photoluminescence Sensing and DFT Analysis of Cd^{2+} Quenching

Chiayee Salih Ajaj[1] | Diyar Sadiq[2] | Shinwar A. Idrees[3] | Carlos J. Tavares[4] | Ahmad Telfah[5,6]

[1]Department of Physics, College of Science, the University of Zakho, Kurdistan Region, Iraq | [2]Scientific Research Center, Duhok Polytechnic University, Duhok, Kurdistan Region, Iraq | [3]Department of Chemistry, College of Science, the University of Zakho, Kurdistan Region, Iraq | [4]Physics Centre of Minho and Porto Universities (CF-UM-UP), University of Minho, Guimarães, Portugal | [5]Fachhochschule Dortmund University of Applied Sciences and Arts, Dortmund, Germany | [6]Cell Therapy Center, The University of Jordan, Amman, Jordan

Correspondence: Chiayee Salih Ajaj (chiayee.ajaj@uoz.edu.krd)

Received: 21 July 2025 | **Revised:** 26 September 2025 | **Accepted:** 15 October 2025

Funding: The authors received no specific funding for this work.

Keywords: carbon quantum dots | Cd^{2+} | photoluminescence | sunflower seed shell

ABSTRACT

This study introduces the synthesis, characterization, and utilization of carbon quantum dots (CQDs) from sunflower seed shells for the first time, specifically as a photoluminescence (PL) sensor for cadmium ion detection. CQDs were synthesized by a hydrothermal method. The CQDs were analyzed employing various physicochemical methods, including XRD, FTIR, TEM, UV–Vis spectroscopy, and fluorescence spectroscopy. The green-source CQDs demonstrated an average nanoscale dimension of 2.1 nm and displayed PL behavior, an emission peak at 497 nm, with a quantum yield (QY) of 33.5%. The synthesized CQDs exhibited significant selectivity for Cd^{2+} ion detection, with PL intensity diminishing as Cd^{2+} concentrations increased (1–10 μM). The detection limit was established at 0.12 μM, while the limit of quantification was set at 0.38 μM. Selectivity experiments demonstrated that the CQDs displayed a robust response to Cd^{2+} ions with negligible interference from other metal ions. The results indicate that the synthesized CQDs are a viable, economical, and eco-friendly material for the detection of cadmium contamination in water. Additionally, density functional theory (DFT) measurements were employed to investigate the quenching mechanism between CQDs and Cd^{2+} ions. The findings indicated that aldehyde groups on the CQD surface demonstrate the most robust interaction with Cd^{2+} ions, elucidating the fluorescence quenching mechanism.

1 | Introduction

In contemporary nanotechnology, the transformation of agricultural waste into high-value nanomaterials presents an effective "waste-to-wealth" strategy. Over the past decade, developing countries have faced persistent challenges with soil and land pollution [1–3]. Biomass waste, including agricultural residues and food processing byproducts, has been identified as a significant environmental contaminant. To mitigate these concerns, carbon quantum dots (CQDs) have been synthesized from various natural solid waste materials, such as orange peels, coffee grounds, sugarcane, watermelon peels, cabbage, tamarind, pomelo peels, pineapple peels, lemon peels, papaya, and potatoes, following green chemistry principles [4–6].

© 2025 John Wiley & Sons Ltd.

CQDs are a novel class of nanomaterials that are highly regarded for their distinctive optical features, chemical stability, and low toxicity [7–9]. Their exceptional characteristics have enabled widespread applications in biomedicine (drug delivery, bioimaging), fluorescent inks, sensors, and photocatalysis [10–17]. Progress in CQDs synthesis has concentrated on enhancing optical characteristics through the utilization of various preparation and manufacturing techniques. Various methods, such as laser ablation, arc discharge, solvothermal oxidation, hydrothermal treatment, and microwave irradiation [18, 19], have been utilized to synthesize CQDs from both synthetic and natural carbon sources. Among these, hydrothermal synthesis using biomass waste offers distinct advantages—cost reduction, process simplicity, readily available precursors, and low toxicity—making it an attractive approach for sustainable nanomaterial development [20, 21]. Hydrothermal carbonization is regarded as an efficient, environmentally sustainable, and economical process for the manufacture of CQDs under mild experimental circumstances, adhering to the principles of green chemistry [22].

The application of CQDs as fluorescent detectors for the detection of metal ions is an innovative approach to addressing environmental and health hazards. Industrial effluents containing toxic heavy metals severely contaminate surface and groundwater, posing risks to human health and ecosystems [23, 24]. While certain metal ions, such as zinc (Zn^{2+}) and iron (Fe^{2+}), are essential for metabolic functions in controlled concentrations, others, including mercury (Hg^{2+}), lead (Pb^{2+}), and cadmium (Cd^{2+}), exhibit high toxicity even at trace levels [25, 26].

Among these, cadmium (Cd^{2+}) is particularly hazardous due to its widespread industrial utilization in plastic pigmentation, cigarette manufacturing, and nickel-cadmium batteries. Cd^{2+} is highly mobile in plants, disrupting cell membranes, biomolecules, and organelles, ultimately impairing plant metabolism. In contrast to necessary metals, cadmium has no known biological function and poses severe risks to living organisms due to bioaccumulation. Prolonged exposure can cause kidney damage, lung disease, and increased risks of prostate and lung cancers in humans [23].

In the current study, we conduct a thorough examination of the biosynthesis of CQDs from sunflower seed shells using a hydrothermal technique. This study highlights the manufacture and application of a very selective fluorescence sensor for Cd^{2+} ions. This study represents a novel contribution to the area, as no prior research has investigated the application of sunflower seed shell-derived CQDs for Cd^{2+} detection using photoluminescence (PL) quenching.

2 | Experimental Part

2.1 | Materials and Instruments

Samples of sunflower seed shells were collected from sunflower seeds used as food. This research was carried out in Mserike (36.87 N, 42.8 E), located in the Duhok, Kurdistan region of Iraq. As they satisfied the required reagent quality standards, no further purification was necessary prior to use. Distilled water had been produced in the chemical analysis laboratory.

The synthesized sunflower seed shell carbon quantum dots (SCQDs) were characterized utilizing different characterization techniques. Transmission electron microscopy (TEM) was conducted utilizing a TEC9G20 (FEI, United States), at a voltage gradient of 200 kV [27]. PL was conducted utilizing a custom-designed luminescence spectroscopy from Canada (SCIENTECH 9702). A high-resolution X-ray diffraction (HR-XRD) examination was performed utilizing a PAN X-Pert apparatus (United Kingdom). Fourier transform infrared (FTIR) spectroscopy has been obtained utilizing Thermo Scientific equipment from the United States. The UV–Vis study was conducted utilizing a CECIL CE 7200 spectrum analyzer, covering a wavelength range of 190–900 nm. An energy-dispersive X-ray spectroscopy (EDX) was conducted with a QUANTA 450 from Carl Zeiss AG (Supra 55VP). A KT7-900-434 extremely fast centrifuge (Heller International Marketing Co. Ltd., Germany) was utilized for the preparation of the samples. Secondary instruments comprised an ultrasonic cleaner (DW-120D, China), an AL104 electronic balance (Mettler Toledo, China), and an extremely high-temperature muffle furnace (DRAWELL, China).

2.2 | Synthesis of SCQDs

The preparation of SCQDs was conducted utilizing a one-pot hydrothermal technique, as demonstrated in Figure 1. The sunflower seed shells were first fragmented and mixed with distilled water, then filtered using a paper filter. The mixture was subjected to centrifugation at 8500 rpm for 10 min. Next, 1 g of the filtered sunflower seed shell was mixed with 55 mL of distilled water and stirred. The resulting mixture was transferred into a 200 mL Teflon-lined autoclave and heated at 200°C for 15 h using a hydrothermal process. After cooling to ambient temperature, the obtained brown solution has been centrifuged at 12,000 rpm for 15 min to remove residual impurities. The final product was freeze-dried before further characterization and analysis.

2.3 | Measurement of Quantum Yield (QY)

The QY of CQDs obtained from sunflower seed shells was evaluated, using Rhodamine B as a reference standard. The QY of the SCQDs in a solution of water was determined using Equation (1) presented below:

$$Q.Y_{CQDs} = Q_R * \frac{I_{CQDs}}{I_R} * \frac{A_R}{A_{CQDs}} * \frac{n^2{}_{Sample}}{n^2{}_R} \quad (1)$$

where Q_R denotes the quantum yield of the reference (rhodamine B, with a value of 0.31), I_{CQDs} represents the maximum intensity of CQDs, I_R signifies the maximum intensity of the reference, A_R indicates the maximum absorption of the reference, A_{CQDs} refers to the maximum absorption of CQDs, and n is the refractive index of both samples (water). The quantum yield of SCQDs is at an excitation wavelength of 370 nm [24].

15227243, 2025, 11, Downloaded from https://analyticalsciencejournals.onlinelibrary.wiley.com/doi/10.1002/bio.70347 by Universidade Do Minho, Wiley Online Library on [28/11/2025]. See the Terms and Conditions (https://onlinelibrary.wiley.com/terms-and-conditions) on Wiley Online Library for rules of use; OA articles are governed by the applicable Creative Commons License



FIGURE 1 | A schematic illustration depicting the preparation of SCQDs from sunflower seed shells.

2.4 | Detection of Cd^{2+} Ions

The quantification of Cd^{2+} was performed in an aqueous solution. In a typical experimental setup, stock solutions of Cd^{2+} ions at a concentration of 100 mM were prepared by dissolving and diluting cadmium salts in distilled water. To determine the Cd^{2+} concentration, various solutions with different cadmium concentrations were mixed with a fixed volume of 1.0 mL of SCQD solution. The fluorescence spectra were recorded at 2-min intervals.

2.5 | Computational Simulation

To investigate the quenching sites on the surface of the synthesized SCQDs, a single-layer graphite sheet containing hydroxyl, carboxyl, and aldehyde functional groups was modeled. The structure was then optimized, and its binding energy, optical properties, and electronic properties were analyzed using density functional theory (DFT) with pseudopotential methods based on a plane wave. For this reason, Quantum Espresso, BURAI, MS, and Excel software were applied. The computations were carried out using the GGA/PBE functional. The computational parameters were set as follows: an energy cut-off of 489.8 eV, Brillouin zone integration using a $1\times1\times1$ k-point Monkhorst-Pack grid, and an SCF tolerance of 1×10^{-6} eV/atom.

3 | Findings and Discussion of SCQDs

3.1 | Characterization and Analyses

The crystallinity of the prepared SCQDs was investigated using XRD, as shown in Figure 2A. The extensive XRD pattern displays significant diffraction peaks around 22.1° and 42.7°, corresponding to the (002) and (100) planes of the graphitic arrangement, signifying the amorphous nature of SCQDs. The d-spacing of the SCQDs was ascertained utilizing Bragg's equation and was found to be 4.00 Å and 2.11 Å, respectively. Notably, the d-spacing of 4.00 Å is significantly larger than the typical 3.35 Å observed in well-ordered graphite [25]. This suggests that the SCQDs may possess a turbostratic carbon structure [27, 28].

The chemical constitution of the SCQDs was analyzed via EDX spectroscopy, as indicated in Figure 2B. The EDX spectrum confirms the amount of carbon (C) (82.3%) and oxygen (O) (14.3%), consistent with the expected chemical composition derived from sunflower seed shells. The additional presence of Au and Cu in the spectrum is due to the gold coating and copper holder used for sample preparation. The EDX results reveal a higher concentration of carbon compared to oxygen, suggesting that the SCQDs are primarily composed of carbon, with a significant level of oxygen-based functional groups [26]. The increased oxygen content indicates a higher degree of surface oxidation, which provides reactive sites that may enhance the SCQDs' reactivity.

Imaging was employed to observe the morphology of SCQDs. As depicted in Figure 2C, the SCQDs are spherical and well-dispersed in water, with no visible aggregation. The TEM image also reveals a lattice spacing of 2.40 Å; this corresponds to the spacing of lattice structures seen in graphitic carbon atoms [29]. The size distribution histogram in Figure 2D indicates that the mean nanoscale dimension of the SCQDs is around 2.1 nm ± 0.4, confirming their small size and uniform distribution.

FTIR spectroscopy was employed to analyze the surface chemistry and functional groups of the synthesized SCQDs. As depicted in Figure 3A, the FTIR spectrum exhibits a broadened peak at 3313 cm^{-1}, which corresponds to the repetitive vibrations of the O—H functional group. Additional peaks at 2159, 1636, and 469 cm^{-1} correspond to the vibrations of C═C, C—O (carboxyl), and C—H groups, respectively, present in the SCQDs. The peak values signify the existence of diverse organic functional groups, including —OH, —C—O, and —C—H, on the top layer of the SCQDs. FTIR measurement verifies the existence of hydroxyl and carbonyl functionalities, indicating that these compounds are essential to the surface chemistry of the SCQDs.

The Raman spectra for SCQDs display distinct carbon peaks at 1381 and 1640 cm^{-1}, which relate to the D-band and G-band, respectively, as illustrated in Figure 3B. The D-band corresponds to sp3 carbons, formed by structural defects like dangling bonds and disordered graphite, whereas the G-band relates to sp2-hybridized graphitic carbons, signifying the vibrations that occur in the graphitic lattice of carbon atoms arranged in

15227243, 2025, 11, Downloaded from https://analyticalsciencejournals.onlinelibrary.wiley.com/doi/10.1002/bio.70347 by Universidade Do Minho, Wiley Online Library on [28/11/2025]. See the Terms and Conditions (https://onlinelibrary.wiley.com/terms-and-conditions) on Wiley Online Library for rules of use; OA articles are governed by the applicable Creative Commons License

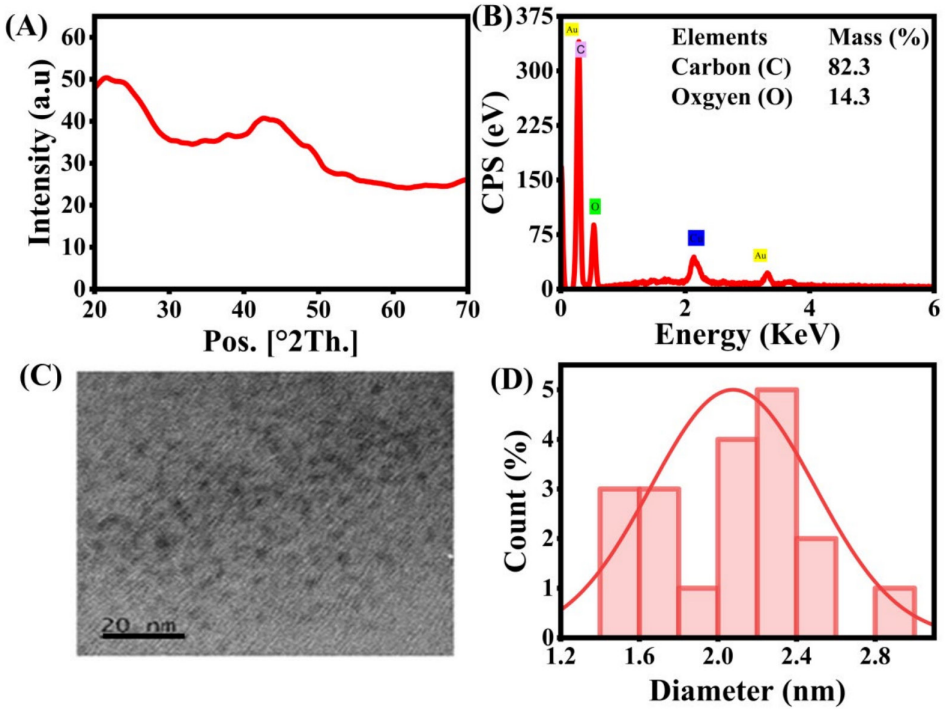


FIGURE 2 | (A) XRD pattern of SCQDs, (B) EDX of SCQDs, (C) TEM morphology of SCQDs, and (D) histogram showing the component size spacing among semiconductor quantum dots synthesized of SCQDs.

a two-dimensional hexagonal structure. The intensity ratio of the D-band relative to the G-band (I_D/I_G) among the SCQDs has been determined to be 1.2. This high ratio signifies a highly disordered structure, characterized by substantial functionalization and the integration of heteroatoms, hence increasing the proportion of sp3 carbons [30]. The Raman study indicates that the SCQDs exhibit significant amorphousness, confirming the XRD findings. The D-band corresponds to the vibrations of carbon atoms having dangling bonds in disordered regions, whereas the G-band signifies the vibrations of sp2-bonded carbon atoms.

Optical properties were studied using UV–Vis and fluorescence spectroscopy. Figure 3C shows the UV–Vis absorption spectra of the SCQDs, which exhibit a broad and sharp peak at 280 nm, corresponding to the $\pi \rightarrow \pi^*$ transitions. The UV–Vis results propose that oxygen-based functional groups, along with C═C sp^2 carbon domains, are present in the SCQDs [31]. The inset of Figure 3D displays the appearance of the diluted SCQDs solution, which appears light brown under visible light but turns bright blue when exposed to fluorescent UV light at 365 nm. This confirms the UV–Vis analysis and supports the successful synthesis of SCQDs from sunflower seed shells.

The fluorescence spectra of SCQDs ranging from 380 to 450 nm are presented in Figure 3E. The intensity of the fluorescence reaches its maximum at an excitation wavelength of 420 nm, with peak emission detected at 497 nm. As the excitation wavelength increases, the emission peaks undergo a red shift, initially causing an elevation in fluorescence intensity, followed by a slight decrease. These results indicate that the SCQDs exhibit emission characteristics that are dependent on the excitation wavelength. That conduct can be ascribed to the diverse surface organic groups present on the SCQDs [28]. The luminescence characteristics of the SCQDs can be attributed to the red edge operation, aromatic conjugated frameworks, emissive traps, nanoparticle size, and surface chemistry, influenced by the presence of oxygen groups with functional properties [26].

3.2 | Quantum Yield of SCQDs

The QY has been calculated for SCQDs. The UV–vis spectra of SCQDs and rhodamine B have been measured experimentally, as illustrated in Figure 4A. The photoluminescence spectra of SCQDs and rhodamine B were successfully determined, as seen in Figure 4B. All samples dissolved in distilled water created solutions with comparable refractive indices. The experimental analysis of the QY of SCQDs, according to Equation (1), produced values of 33.5%.

3.3 | Effect of pH

The pH sensitivity of SCQD nanoparticles is a crucial factor in their potential applications in intelligent sensing and detection, particularly due to their remarkable fluorescence properties. To investigate the impact of pH on the detection capability of SCQDs, the PL of SCQDs was assessed at varying pH levels (3, 5, 6, 7, 8, 10, 12, and 14), as depicted in Figure 5A. The PL intensity rises as the pH increases from 3 to 6 but progressively diminishes as the pH shifts from 6 to 14, indicating that the as-prepared SCQDs are highly sensitive to both acidic and basic conditions [27]. The maximum luminescence intensity was recorded at pH = 6, meaning it is deemed the ideal environment to operate a sensing tool aimed at metal ions [26]. This characteristic also suggests the potential use of SCQDs in bioimaging and sensor applications. In the examination of fluorescence detection for

15227243, 2025, 11, Downloaded from https://analyticalsciencejournals.onlinelibrary.wiley.com/doi/10.1002/bio.70347 by Universidade Do Minho, Wiley Online Library on [28/11/2025]. See the Terms and Conditions (https://onlinelibrary.wiley.com/terms-and-conditions) on Wiley Online Library for rules of use; OA articles are governed by the applicable Creative Commons License

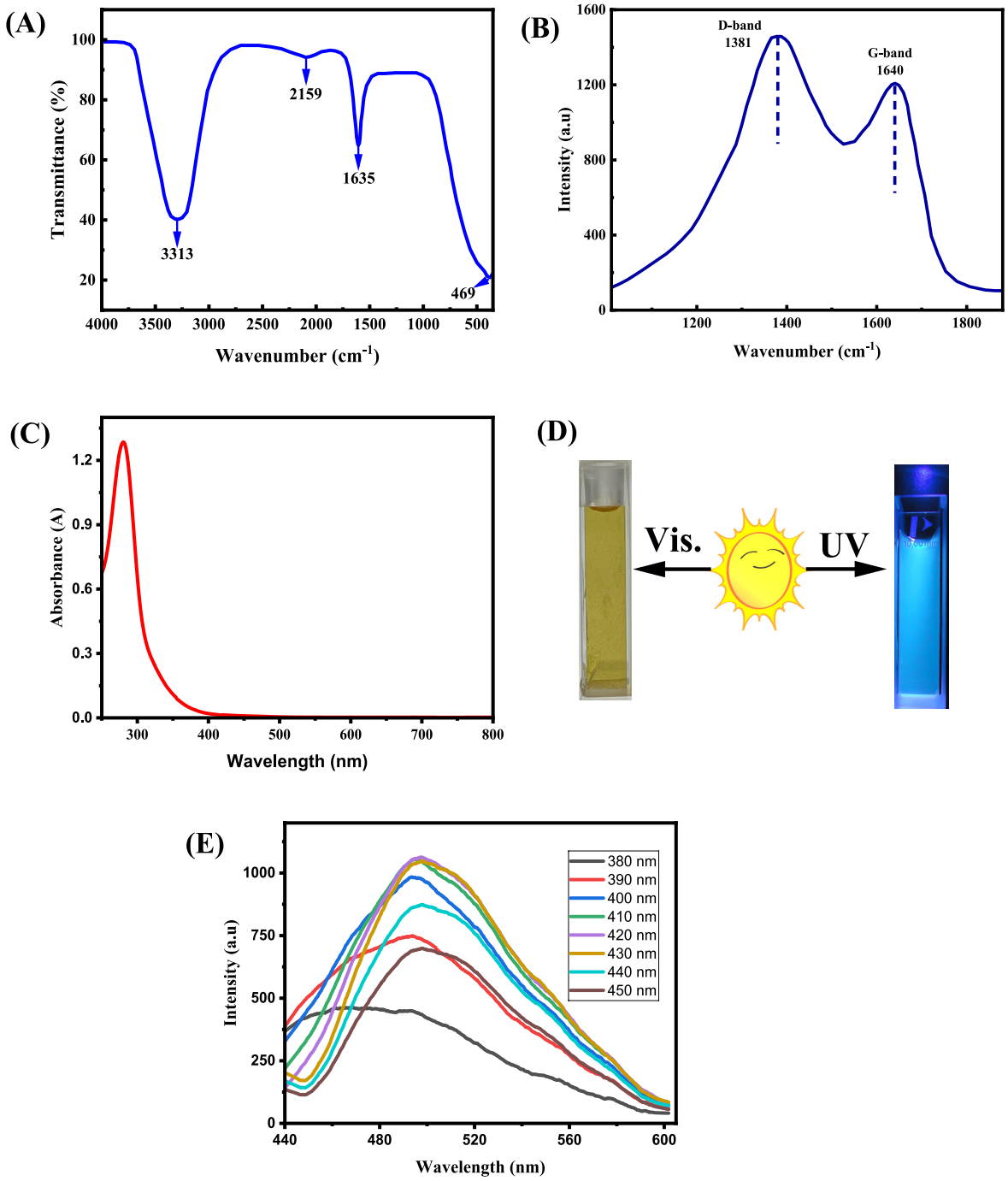


FIGURE 3 | (A) FTIR spectrum of SCQDs, (B) Raman shift of SCQDs, (C) UV–Vis absorbing spectrum of SCQDs, (D) SCQDs illuminated by visible light (left) and ultraviolet light (right), and (E) PL of SCQDs at different excitation wavelengths, spanning from 380 to 450 nm.

metal ions, variations in fluorescence intensity were monitored as an objective of pH [32]. The changes seen in the amount of fluorescence can be ascribed to substantial modifications in the surface functionalities of the SCQDs, produced by H^+ or OH^- ions. The interaction of H^+ ions results in the protonation process of the outer groups, while OH^- ions deprotonate the surface groups, transforming them to COO^- and O^-, respectively. These changes cause the observed variations in fluorescence intensity, as depicted in Figure 5B. The findings indicate that the developed SCQDs are very appropriate for application as an excellent quality pH illumination sensor [33]. This variation of pH sensitivity is likely attributed to the gain and donation of protons due to the functional groups present on the surfaces of the SCQDs [39, 40].

3.4 | Detection of Cd^{2+}

The selectivity detection of metal ions using agricultural waste-derived luminescent SCQDs was applied to diverse metallic cations, including Ag^{2+}, Ca^{2+}, Mg^{2+}, Fe^{3+}, Ni^{2+}, Co^{2+}, Zn^{2+}, Hg^{2+}, Cu^{2+}, Pb^{2+}, Ba^{2+}, Cr^{3+}, K^+, Na^+, Cl^-, SO_4^{2-}, NO_3^-, and Cd^{2+}, as shown in Figure 6A. From the analysis of the data, it was observed that Cd^{2+} ions exhibited a notable

15227243, 2025, 11, Downloaded from https://analyticalsciencejournals.onlinelibrary.wiley.com/doi/10.1002/bio.70347 by Universidade Do Minho, Wiley Online Library on [28/11/2025]. See the Terms and Conditions (https://onlinelibrary.wiley.com/terms-and-conditions) on Wiley Online Library for rules of use; OA articles are governed by the applicable Creative Commons License

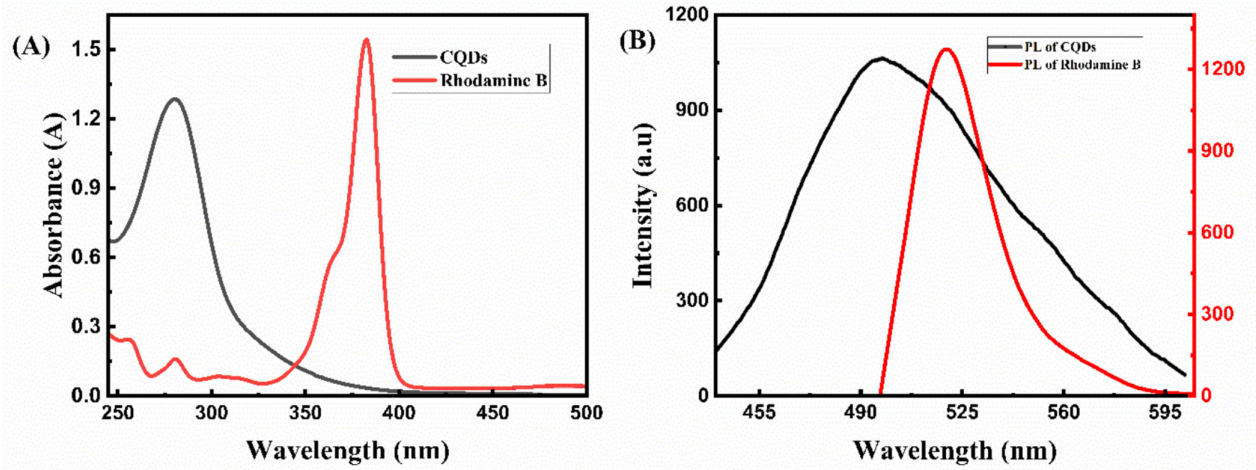


FIGURE 4 | QY of SCQDs, (A) UV–Vis of SCQDs and rhodamine B and (B) PL of SCQDs and rhodamine B.

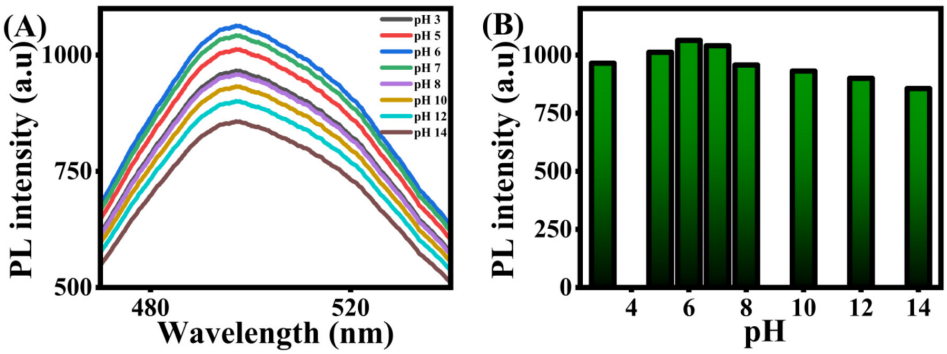


FIGURE 5 | Impact of pH on the illumination intensity of SCQDs. (A) The luminescence intensity at various pH values. (B) Correlation between luminescence intensity and pH.

response, with an increase in the fluorescence quenching signal $(F_0 - F)/F_0$ [34]. As illustrated in Figure 6B, the fast quench of fluorescence is ascribed to the effective interaction of energy involving Cd^{2+} ions and the surface groups of the SCQDs. The fluorescence reaction of the SCQDs solution was evaluated with several metal ions, each at a constant concentration of 100 mM, utilizing the wavelength of excitation of 370 nm. The PL intensity was evaluated over a range of Cd^{2+} ion concentrations (from 1 to 10 μM), demonstrating an opposite correlation between fluorescence intensity and Cd^{2+} quantity, as illustrated in Figure 6C.

The presence of Cd^{2+} ions significantly diminished the fluorescence of the SCQDs. The decrease in fluorescence is due to the chemical reaction between Cd^{2+} ions and functional groups that contain oxygen on the SCQD surface. The chemical reaction presumably caused SCQD aggregation, which subsequently led to the quenching of fluorescence [35]. The quenching performance was assessed with the Stern–Volmer equation [36].

$$\frac{F_0}{F} = 1 + K_{SV} * [Q] \tag{2}$$

where K_{SV} is the Stern-Volmer quenching constant, $[Q]$ is the concentration of the analytical agent, F_0 represents the fluorescence intensity without Cd^{2+}, and F represents how much fluorescence occurs in an amount of Cd^{2+}. The limit of detection (LOD) has been identified using the equation $LOD = 3S/q$, where S denotes the standard deviation and q indicates the slope of the calibration curve illustrated in Figure 6D. A linear association ($R^2 = 0.9981$) was detected across an amount range of 1–10 μM, as depicted in Figure 6D. The LOD was determined to be 0.12 μM, while the limit of quantification (LOQ) has been found to be 0.38 μM. A brief overview of various detection techniques for cadmium quantification is shown in Table 1. The results demonstrate that luminous SCQDs obtained from bio-waste have been particularly efficient for detecting Cd^{2+} in aquatic environments.

3.5 | Mechanism Exploration With DFT

The calculations using DFT were conducted to investigate the quenching interaction between SCQDs and Cd^{2+} ions. Characterization results indicated that SCQDs surfaces primarily consist of graphite carbon with oxygen-based functional groups, including carboxyl, aldehyde, and alcohol. Binding energy analysis revealed that all these groups interacted with Cd^{2+}, but the aldehyde group exhibited the strongest interaction. Subsequent calculations focused on electronic structure and optical properties based on this interaction.

Figure 7A,C presents the band structure, while Figure 7B,D illustrates the TDOS before and after quenching. The results

15227243, 2025, 11, Downloaded from https://analyticalsciencejournals.onlinelibrary.wiley.com/doi/10.1002/bio.70347 by Universidade Do Minho, Wiley Online Library on [28/11/2025]. See the Terms and Conditions (https://onlinelibrary.wiley.com/terms-and-conditions) on Wiley Online Library for rules of use; OA articles are governed by the applicable Creative Commons License

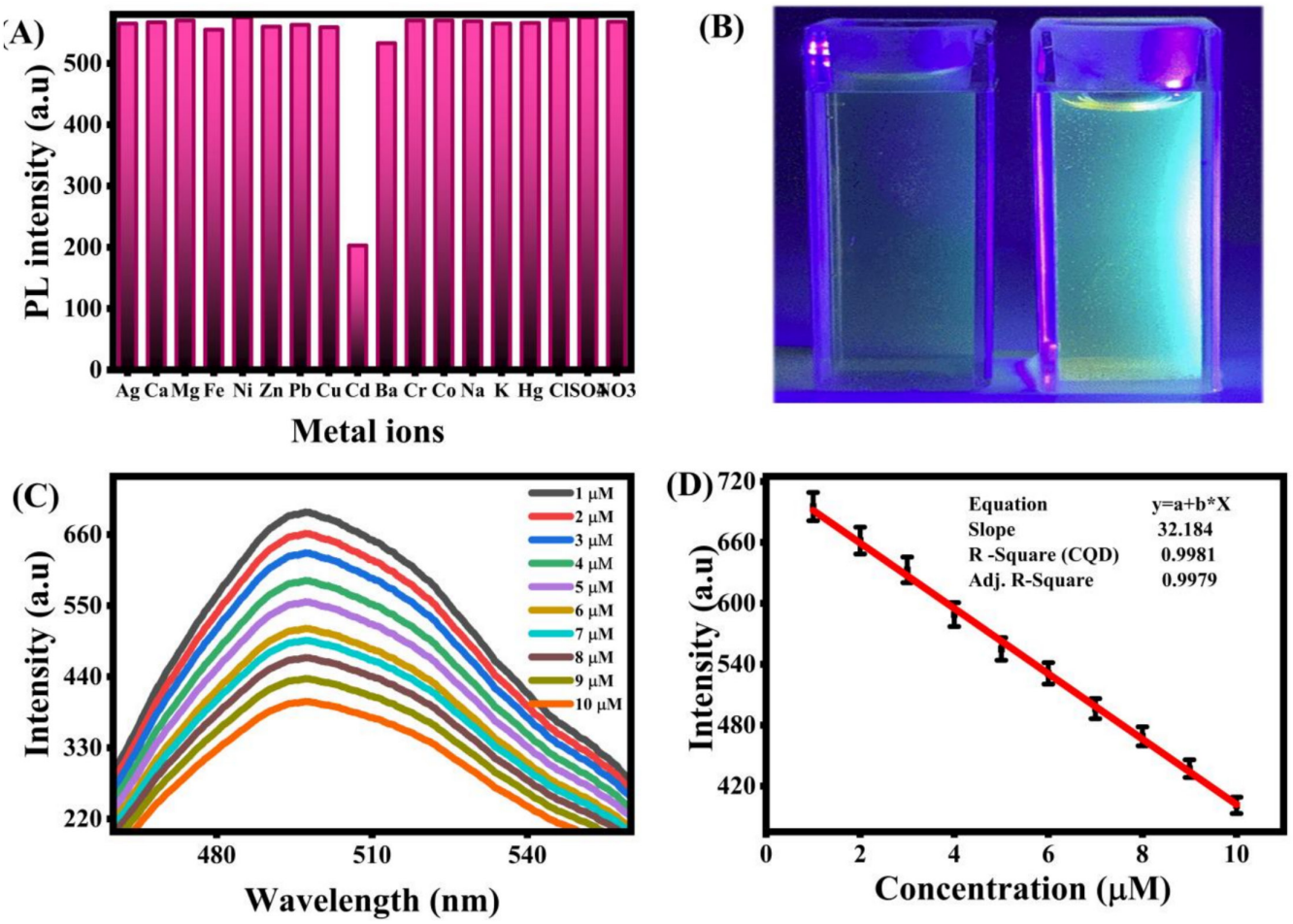


FIGURE 6 | (A) The influence of different ions on the fluorescent attributes of SCQDs. (B) Fluorescence images for SCQDs solution before (right) and after the introduction of Cd^{2+} ions (left). (C) Change of luminescence intensity of SCQDs with different amounts of Cd^{2+} ions. (D) Correlation between PL intensity of SCQDs and Cd^{2+} ion concentration.

TABLE 1 | Comparison of SCQD-based sensors for Cd^{2+} ion detection.

Sensor	LOD [μM]	Linear range [μM]	Ref.
Urea and citric acid	2.21 μM	5.62–5620	[37]
2-amino-3-hydroxypyridine and sodium borohydride	0.45 μM	2.5–22.5	[38]
o-Phosphorylethanolamine and citric acid	0.16 μM	0.5–12.5	[39]
Biomass (sunflower seed shell)	0.12 μM	1–10	This work

indicate an increased number of bands at the Fermi energy level in quenched SCQDs, resulting in a narrower gap between bands. The reduction of the quantity of electronic transitions at the Fermi energy level following Cd^{2+} adsorption confirms that quenching alters the SCQDs' electronic structure, affecting conductivity and PL. Additionally, a reduction in total DOS at the valence band suggests that valence electrons participate in bonding with Cd^{2+}.

HOMO-LUMO energy calculations (Figure 8) revealed an energy gap reduction from 0.29 Ha SCQDs to 0.14 Ha (SCQDs with Cd^{2+}), indicating increased orbital availability due to Cd^{2+} interaction. These values were further used to determine reactivity indices (the ionizing potential, affinity for electrons, electronegativity, chemical potential, chemical hardness, electrophilicity, and nucleophilicity) listed in Table 2. The results suggest that SCQDs are more nucleophilic than SCQDs with Cd^{2+}, supporting their reactivity with cadmium ions. The lower chemical potential of SCQDs before quenching implies electron transfer from SCQDs to Cd^{2+}, leading to reduced fluorescence.

For optoelectronic applications, the optical properties of SCQDs are critical. The energy loss function (Figure 9) shows UV–visible peaks indicative of plasmonic effects that enhance light–matter interactions and improve photosensor sensitivity. A slight shift (2.78–2.48 eV and 10.36–10.45 eV) after Cd^{2+} interaction suggests modifications in electronic transitions rather than

15227243, 2025, 11, Downloaded from https://analyticalsciencejournals.onlinelibrary.wiley.com/doi/10.1002/bio.70347 by Universidade Do Minho, Wiley Online Library on [28/11/2025]. See the Terms and Conditions (https://onlinelibrary.wiley.com/terms-and-conditions) on Wiley Online Library for rules of use; OA articles are governed by the applicable Creative Commons License

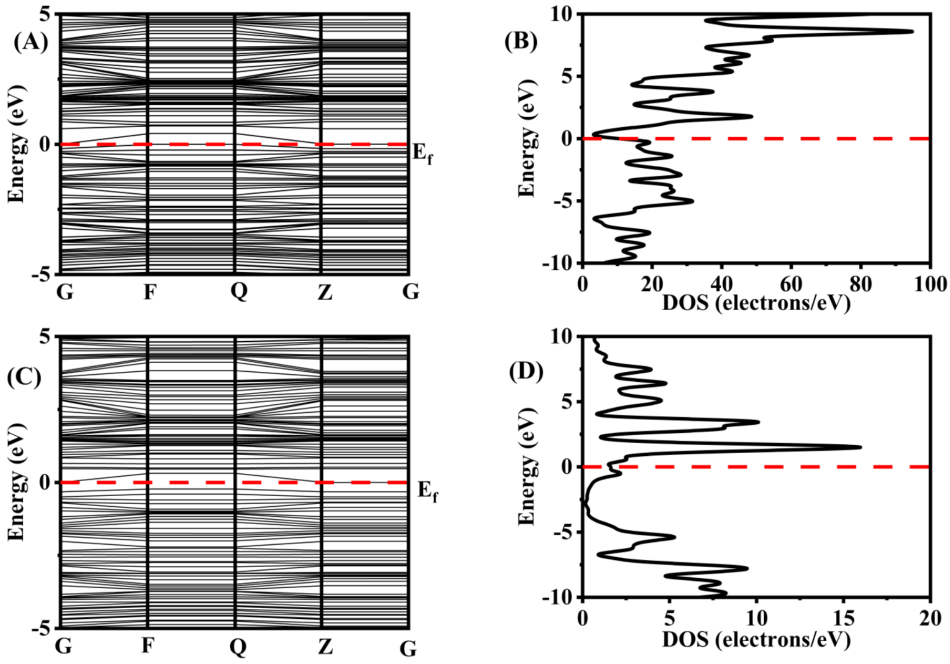


FIGURE 7 | The band structure and additive density of states: (A and B) before quenching, (C and D) after quenching.

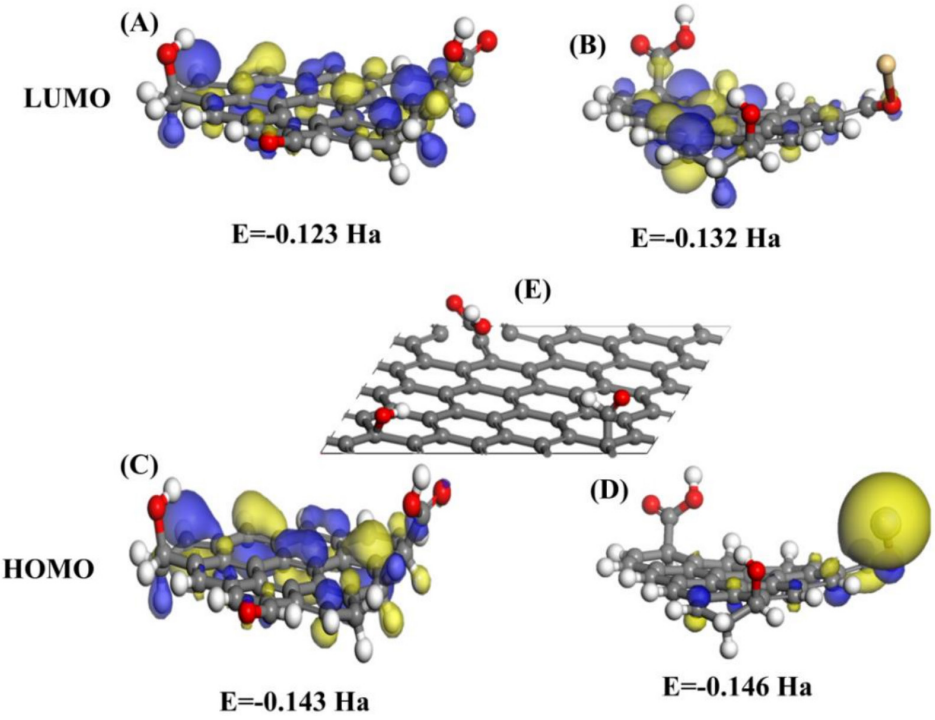


FIGURE 8 | Density distribution of HOMO and LUMO: (A and C) before quenching, (B and D) after quenching, and (E) periodic structure of SCQDs.

bulk structural changes. Reflectivity calculations (Figure 9C,D) show minimal alteration, indicating that quenching is primarily a surface phenomenon.

Optical conductivity analysis (Figure 9E,F) highlights absorption due to electronic transitions in the UV range, with peaks at 5.06 and 5.16 eV. A slight increase in post Cd^{2+} interaction suggests improved charge carrier mobility, correlating with enhanced conductivity. The observed PL reduction further supports non-radiative recombination pathways, diminishing radiative emission and improving charge carrier dynamics.

Our findings align with theoretical predictions and experimental data, demonstrating minor but significant modifications in energy loss, reflection, and conductivity upon Cd^{2+} interaction. The observed peaks in the UV–visible area indicate the existence of plasmonic effects, hence enhancing the potential of SCQDs for photosensor applications.

15227243, 2025, 11, Downloaded from https://analyticalsciencejournals.onlinelibrary.wiley.com/doi/10.1002/bio.70347 by Universidade Do Minho, Wiley Online Library on [28/11/2025]. See the Terms and Conditions (https://onlinelibrary.wiley.com/terms-and-conditions) on Wiley Online Library for rules of use; OA articles are governed by the applicable Creative Commons License

TABLE 2 | Calculated ionization potential (IP), electron affinity (EA), electronegativity (χ), chemical potential (μ), global hardness (η), global electrophilicity index (ω), and global nucleophilicity index (ε) for SCQDs and SCQDs after quenching with Cd^{2+} ions.

Compound	IP	EA	X	μ	H	Ω	E
QDs alone	3.89	3.34	3.615	−4.47	0.275	6.53	0.15
QDs with Cd	3.97	3.59	3.782	−4.87	0.19	7.15	0.13

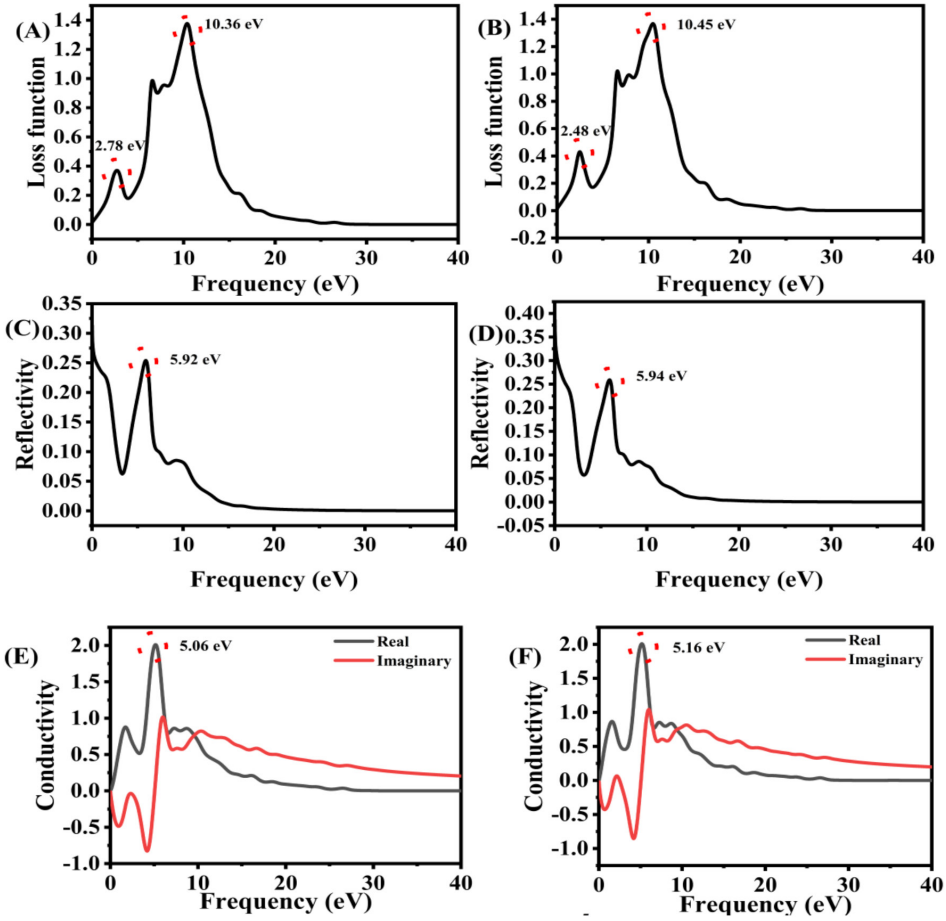


FIGURE 9 | Optical properties spectra: (A and B) loss function, (C and D) reflectivity, and (E and F) conductivity, before and after quenching.

4 | Conclusions

This study presents the synthesis of green SCQDs from sunflower seed shells using a hydrothermal method. The synthesized SCQDs were evaluated for their potential applications as sensors for Cd^{2+} metal ions and pH at room temperature. Morphological analysis, including TEM imaging and XRD, disclosed spherical SCQDs having an average diameter of about 2.07 nm. The SCQDs underwent optical evaluation by UV–Vis, PL, and FTIR spectrum analysis methods. FTIR investigation revealed the existence of functional groups on the surface, involving O—H, C—O, C═C, and C—H. Fluorescence characteristics of the SCQDs were excitation-dependent, exhibiting a maximum emission at 497 nm upon excitation at 420 nm with a maximum QY of 33.5%. These SCQDs demonstrated excellent selectivity and sensitivity for detecting Cd^{2+} ions, possessing a detection limit of about 0.12 μM and a quantification limit around 0.38 μM. Optical robust linear correlations between luminescence intensity and Cd^{2+} quantity (1–10 μM) were found, validating their efficacy as a fluorescence sensor for Cd^{2+} ions. The proposed synthesis method is faster, cost-effective, and environmentally friendly, providing a promising way to enable the synthesis of green luminous SCQDs. The SCQDs have remarkable sensitivity, and minimal detection thresholds for metal ions make them highly effective and biocompatible fluorescent sensors. Additionally, their small size, bright multicolor fluorescence, and biocompatibility suggest broad potential applications in biological, chemical, and physical fields. DFT calculations further revealed that the quenching mechanism between SCQDs and Cd^{2+} ions primarily involves the aldehyde functional group on the SCQD surface, as demonstrated by binding energy and electronic structure calculations.

Conflicts of Interest

The authors declare no conflicts of interest.

15227243, 2025, 11, Downloaded from https://analyticalsciencejournals.onlinelibrary.wiley.com/doi/10.1002/bio.70347 by Universidade Do Minho, Wiley Online Library on [28/11/2025]. See the Terms and Conditions (https://onlinelibrary.wiley.com/terms-and-conditions) on Wiley Online Library for rules of use; OA articles are governed by the applicable Creative Commons License

Data Availability Statement

The data that support the findings of this study are available on request from the corresponding author. The data are not publicly available due to privacy or ethical restrictions.

References

1. S. T and D. Rs, "Green Synthesis of Highly Fluorescent Carbon Quantum Dots From Sugarcane Bagasse Pulp," *Applied Surface Science* 390 (2016): 435–443, https://doi.org/10.1016/j.apsusc.2016.08.106.

2. X. Chai, H. He, H. Fan, X. Kang, and X. Song, "A Hydrothermal-Carbonization Process for Simultaneously Production of Sugars, Graphene Quantum Dots, and Porous Carbon From Sugarcane Bagasse," *Bioresource Technology* 282 (2019): 142–147, https://doi.org/10.1016/j.biortech.2019.02.126.

3. Q. Zhang, X. Zhang, L. Bao, et al., "The Application of Green-Synthesis-Derived Carbon Quantum Dots to Bioimaging and the Analysis of Mercury (II)," *Journal of Analytical Methods in Chemistry* 2019 (2019): 8183134, https://doi.org/10.1155/2019/8183134.

4. K. Chang, Q. Zhu, L. Qi, M. Guo, W. Gao, and Q. Gao, "Synthesis and Properties of Nitrogen-Doped Carbon Quantum Dots Using Lactic Acid as Carbon Source," *Materials* 15, no. 2 (2022): 466.

5. M. Preethi, C. Viswanathan, and N. Ponpandian, "A Green Path to Extract Carbon Quantum Dots by Coconut Water: Another Fluorescent Probe Towards Fe3+ Ions," *Particuology* 58 (2021): 251–258, https://doi.org/10.1016/j.partic.2021.03.019.

6. Y. Wang and A. Hu, "Carbon Quantum Dots: Synthesis, Properties and Applications," *Journal of Materials Chemistry C* 2, no. 34 (2014): 6921–6939.

7. X. Xu, R. Ray, Y. Gu, et al., "Electrophoretic Analysis and Purification of Fluorescent Single-Walled Carbon Nanotube Fragments," *Journal of the American Chemical Society* 126, no. 40 (2004): 12736–12737.

8. M. Sabet and K. Mahdavi, "Green Synthesis of High Photoluminescence Nitrogen-Doped Carbon Quantum Dots From Grass via a Simple Hydrothermal Method for Removing Organic and Inorganic Water Pollutions," *Applied Surface Science* 463, no. June 2018 (2019): 283–291, https://doi.org/10.1016/j.apsusc.2018.08.223.

9. P. Das, S. Ganguly, S. Mondal, et al., "Heteroatom Doped Photoluminescent Carbon Dots for Sensitive Detection of Acetone in Human Fluids," *Sensors and Actuators B: Chemical* 266 (2018): 583–593, https://doi.org/10.1016/j.snb.2018.03.183.

10. A. Kumari, A. Kumar, S. K. Sahu, and S. Kumar, "Synthesis of Green Fluorescent Carbon Quantum Dots Using Waste Polyolefins Residue for Cu2+ Ion Sensing and Live Cell Imaging," *Sensors and Actuators, B: Chemical* 254 (2018): 197–205, https://doi.org/10.1016/j.snb.2017.07.075.

11. C. Fu, K. Qian, and A. Fu, "Arginine-Modified Carbon Dots Probe for Live Cell Imaging and Sensing by Increasing Cellular Uptake Efficiency," *Materials Science and Engineering C-Materials For Biological Applications* 76 (2017): 350–355, https://doi.org/10.1016/j.msec.2017.03.084.

12. J. Ju and W. Chen, "Synthesis of Highly Fluorescent Nitrogen-Doped Graphene Quantum Dots for Sensitive, Label-Free Detection of Fe (III) in Aqueous Media," *Biosensors & Bioelectronics* 58 (2014): 219–225, https://doi.org/10.1016/j.bios.2014.02.061.

13. T. N. J. I. Edison, R. Atchudan, M. G. Sethuraman, J. J. Shim, and Y. R. Lee, "Microwave Assisted Green Synthesis of Fluorescent N-Doped Carbon Dots: Cytotoxicity and Bio-Imaging Applications," *Journal of Photochemistry and Photobiology, B: Biology* 161 (2016): 154–161, https://doi.org/10.1016/j.jphotobiol.2016.05.017.

14. X. Gao, C. Du, Z. Zhuang, and W. Chen, "Carbon Quantum Dot-Based Nanoprobes for Metal Ion Detection," *Journal of Materials Chemistry C* 4, no. 29 (2016): 6927–6945.

15. J. Ju, R. Zhang, S. He, and W. Chen, "Nitrogen-Doped Graphene Quantum Dots-Based Fluorescent Probe for the Sensitive Turn-On Detection of Glutathione and Its Cellular Imaging," *RSC Advances* 4, no. 94 (2014): 52583–52589.

16. S. C. Nunes, N. J. O. Silva, J. Hümmer, et al., "Water-Mediated Structural Tunability of Alkyl/siloxane Hybrid: From Amorphous to Lamellar Structure or Bilamellar Superstructure," *Journal of Material* 2 (2012): 2087–2099.

17. L. Li, R. Zhang, C. Lu, et al., "In Situ Synthesis of NIR-Light Emitting Carbon Dots Derived From Spinach for Bio-Imaging Applications," *Journal of Materials Chemistry B* 5, no. 35 (2017): 7328–7334.

18. Z. Peng, X. Han, S. Li, et al., "Carbon Dots: Biomacromolecule Interaction, Bioimaging and Nanomedicine," *Coordination Chemistry Reviews* 343 (2017): 256–277, https://doi.org/10.1016/j.ccr.2017.06.001.

19. K. Yang, M. Liu, Y. Wang, et al., "Carbon Dots Derived From Fungus for Sensing Hyaluronic Acid and Hyaluronidase," *Sensors and Actuators B: Chemical* 251 (2017): 503–508, https://doi.org/10.1016/j.snb.2017.05.086.

20. R. Atchudan, T. N. J. I. Edison, K. R. Aseer, S. Perumal, and Y. R. Lee, "Hydrothermal Conversion of *Magnolia liliiflora* Into Nitrogen-Doped Carbon Dots as an Effective Turn-Off Fluorescence Sensing, Multi-Colour Cell Imaging and Fluorescent Ink," *Colloids and Surfaces. B, Biointerfaces* 169, no. March (2018): 321–328, https://doi.org/10.1016/j.colsurfb.2018.05.032.

21. R. Atchudan, T. N. J. I. Edison, S. Perumal, N. Clament Sagaya Selvam, and Y. R. Lee, "Green Synthesized Multiple Fluorescent Nitrogen-Doped Carbon Quantum Dots as an Efficient Label-Free Optical Nanoprobe for In Vivo Live-Cell Imaging," *Journal of Photochemistry and Photobiology, A: Chemistry* 372, no. December 2018 (2019): 99–107, https://doi.org/10.1016/j.jphotochem.2018.12.011.

22. C. Zhao, Y. Jiao, F. Hu, and Y. Yang, "Green Synthesis of Carbon Dots From Pork and Application as Nanosensors for Uric Acid Detection," *Spectrochimica Acta, Part A: Molecular and Biomolecular Spectroscopy* 190 (2018): 360–367, https://doi.org/10.1016/j.saa.2017.09.037.

23. A. K. M. K. Sariga, L. Benny, and A. Varghese, "A Facile, Green Synthesis of Carbon Quantum Dots From *Polyalthia longifolia* and Its Application for the Selective Detection of Cadmium," *Dyes and Pigments* 210, no. August 2022 (2023): 111048, https://doi.org/10.1016/j.dyepig.2022.111048.

24. S. Md Palashuddin and A. Chattopadhyay, "Induction Coil Heater Prepared Highly Fluorescent Carbon Dots as Invisible Ink and Explosive Sensor," *Royal Society of Chemistry* 4 (2014): 31994–31999.

25. C. Thambiliyagodage, S. Nakandala, B. Siriwardana, and B. Lansakara, "One Pot Synthesis of α-Fe2O3/Turbostratic Carbon Composites and Their Photocatalytic Activity Under Sunlight," *Carbon Trends* 5 (2021): 100130, https://doi.org/10.1016/j.cartre.2021.100130.

26. S. Patra, M. Singh, S. Subudhi, et al., "One-Step Green Synthesis of In–Situ Functionalized Carbon Quantum Dots From *Tagetes patula* Flowers: Applications as a Fluorescent Probe for Detecting Fe3+ Ions and as an Antifungal Agent," *Journal of Photochemistry and Photobiology, A: Chemistry* 442 (2023): 114779, https://doi.org/10.1016/j.jphotochem.2023.114779.

27. N. Arumugam and J. Kim, "Synthesis of Carbon Quantum Dots From Broccoli and Their Ability to Detect Silver Ions," *Materials Letters* 219 (2018): 37–40, https://doi.org/10.1016/j.matlet.2018.02.043.

28. L. Gu, J. Zhang, G. Yang, et al., "Green Preparation of Carbon Quantum Dots With Wolfberry as On-Off-On Nanosensors for the Detection of Fe3+ and L-Ascorbic Acid," *Food Chemistry* 376 (2022): 131898, https://doi.org/10.1016/j.foodchem.2021.131898.

29. B. K. John, J. Mathew, S. K, R. E. K, and B. Mathew, "Biomass Derived Carbon Quantum Dots as a Versatile Platform for Fluorescent Sensing, Catalytic Reduction, Fluorescent Ink and Anticancer Agents,"

15227243, 2025, 11, Downloaded from https://analyticalsciencejournals.onlinelibrary.wiley.com/doi/10.1002/bio.70347 by Universidade Do Minho, Wiley Online Library on [28/11/2025]. See the Terms and Conditions (https://onlinelibrary.wiley.com/terms-and-conditions) on Wiley Online Library for rules of use; OA articles are governed by the applicable Creative Commons License

Materials Today Sustainability 26 (2024): 100715, https://doi.org/10.1016/j.mtsust.2024.100715.

30. N. Azam, M. N. Ali, and T. J. Khan, "Carbon Quantum Dots for Biomedical Applications: Review and Analysis," 8 (2021): 1–21.

31. R. Atchudan, T. N. J. I. Edison, S. Perumal, et al., "Concurrent Synthesis of Nitrogen-Doped Carbon Dots for Cell Imaging and ZnO@nitrogen-Doped Carbon Sheets for Photocatalytic Degradation of Methylene Blue," *Journal of Photochemistry and Photobiology A: Chemistry* 350 (2018): 75–85, https://doi.org/10.1016/j.jphotochem.2017.09.038.

32. Y. Zhang, S. Cheng, and Y. Zhang, "Green Fluorescent Carbon Dots for Sensing of Quercetin and pH and Cell Imaging," *Luminescence* 39 (2024): e4638, https://doi.org/10.1002/bio.4638.

33. H. Ma, L. Guan, M. Chen, et al., "Synthesis and Enhancement of Carbon Quantum Dots From Mopan Persimmons for Fe3+ Sensing and Anti-Counterfeiting Applications," *Chemical Engineering Journal* 453 (2023): 139906.

34. G. M. Alshammari, M. S. Al-Ayed, M. A. Abdelhalim, L. N. Al-Harbi, A. A. Qasem, and M. Abdo Yahya, "Development of Luminescence Carbon Quantum Dots for Metal Ions Detection and Photocatalytic Degradation of Organic Dyes From Aqueous Media," *Environmental Research* 226 (2023): 115661, https://doi.org/10.1016/j.envres.2023.115661.

35. D. Wang, Y. Zhang, Z. Cai, et al., "Corn Stalk-Derived Carbon Quantum Dots With Abundant Amino Groups as a Selective-Layer Modifier for Enhancing Chlorine Resistance of Membranes," *ACS Applied Materials & Interfaces* 13, no. 19 (2021): 22621–22634.

36. C. Falco, N. Baccile, and M. M. Titirici, "Morphological and Structural Differences Between Glucose, Cellulose and Lignocellulosic Biomass Derived Hydrothermal Carbons," *Green Chemistry* 13, no. 11 (2011): 3273–3281.

37. L. Li, D. Liu, A. Shi, and T. You, "Simultaneous Stripping Determination of Cadmium and Lead Ions Based on the N-Doped Carbon Quantum Dots-Graphene Oxide Hybrid," *Sensors and Actuators B: Chemical* 255 (2018): 1762–1770, https://doi.org/10.1016/j.snb.2017.08.190.

38. Z. Yan, W. Yao, K. Mai, et al., "A Highly Selective and Sensitive "On-Off" Fluorescent Probe for Detecting Cadmium Ions and L-Cysteine Based on Nitrogen and Boron Co-Doped Carbon Quantum Dots," *RSC Advances* 12, no. 13 (2022): 8202–8210.

39. L. Lin, Y. Wang, Y. Xiao, and W. Liu, "Hydrothermal Synthesis of Carbon Dots Codoped With Nitrogen and Phosphorus as a Turn-On Fluorescent Probe for Cadmium (II)," *Microchimica Acta* 186, no. 3 (2019): 147.

15227243, 2025, 11, Downloaded from https://analyticalsciencejournals.onlinelibrary.wiley.com/doi/10.1002/bio.70347 by Universidade Do Minho, Wiley Online Library on [28/11/2025]. See the Terms and Conditions (https://onlinelibrary.wiley.com/terms-and-conditions) on Wiley Online Library for rules of use; OA articles are governed by the applicable Creative Commons License